Dalton Transactions

ROYAL SOCIETY OF CHEMISTRY

PAPER

View Article Online
View Journal

Cite this: DOI: 10.1039/d1dt01558c

Towards understanding the magnetism of Os(IV) complexes: an *ab initio* insight†

Liviu Ungur, *[a] Katharina Pallitsch, [b] Zeid A. AlOthman, [c] Abdullah A. S. Al-Kahtani,[c] Vladimir B. Arion [d] and Liviu F. Chibotaru *[e,c]

Received 13th May 2021,
Accepted 7th August 2021

DOI: 10.1039/d1dt01558c

rsc.li/dalton

The magnetism of a recently synthesized *trans*-[$Os^{IV}Cl_4(\kappa N_1$-Hind)$_2$] complex ($5d^4$-system), where Hind = 2*H*-indazole, was studied experimentally and theoretically. Relativistic CASSCF/CASPT2 calculations for this and model $[Os^{IV}Cl_6]^{2-}$ complexes were employed to understand the nature of the low-lying multiplets. It is found that despite strong metal–ligand covalency they are basically characterized by the total angular pseudo-momentum $\tilde{J}$ originating from the spin–orbit coupling of the ground-state spin $S = 1$ with the orbital pseudo-momentum $\tilde{L} = 1$ of the Os^{IV} ion. The strong spin–orbit interaction also preserves the dominant $\tilde{J} = 0$ character of the non-magnetic ground state in the *trans*-[$Os^{IV}Cl_4(\kappa N_1$-Hind)$_2$] complex despite significant deviation of the ligand environment of Os^{IV} from octahedral symmetry. At the same time the spin–orbit admixture of all multiplets arising from the t_{2g}^4 strong-field electronic configuration is indispensable for the correct description of magnetic properties of Os^{IV} complexes. Moreover, based on *ab initio* calculations, we argue that the charge-transfer states play an important role in the magnetism of the present and probably other 5d complexes, a situation never encountered for 3d and 4f compounds.

1 Introduction

Recently, 4d and 5d metal ions have received growing attention due to their various properties ranging from anticancer agents,[1,2] towards catalytic,[3,4] optic[5] and magnetic properties.[6] The interplay between ligand field and spin–orbit coupling effects has led to exotic quantum phenomena such as spin–orbit liquid states with high magnetic ordering temperatures and high-temperature superconductivity.[7–11] From the point of view of magnetic properties, these metal ions offer two significant advantages. First, they possess a strong spin–orbit coupling, much larger than the 3d metals and comparable in strength with lanthanides and actinides.[12] Strong spin–orbit coupling in the latter allowed for the observation of blocking of magnetisation in mononuclear lanthanide[13–21] and actinide[22,23,24] complexes, making them single-molecule magnets (SMM). The necessary condition for the SMM behaviour of these mononuclear complexes is the efficient coupling of the spin momentum to the orbital momentum. The orbital momentum is usually strongly suppressed in transition metal complexes.[25] It may become unquenched either due to strong spin–orbit coupling on the metal ion, counteracting the quenching effect of low-symmetry crystal field or at sufficiently high symmetry of the complex. As an example of the latter situation, the SMM behaviour was found in Fe(II) pyrrolide complexes with a geometry close to trigonal symmetry.[26] On the other hand, for the 4d metal ions, the unquenched orbital momentum can arise in complexes without point group symmetry. For example, large deviations of the g factors from 2 have been found for low-symmetry fragments of $[Mo(CN)_7]^{4-}$ by *ab initio* calculations.[27] A second advantage of 4d and 5d metal ions is their larger radii compared to the 3d ions allowing for stronger overlap with the ligand's orbitals and, therefore, for much stronger exchange interaction with neighbouring metal sites in polynuclear compounds.[28] This enables the design of magnetic networks combining strong magnetic anisotropy with magnetic ordering at high Curie temperature, as achieved, *e.g.*, in antiferromagnetically coupled Mo–Mn cyano-bridged networks based on heptacyanomolybdate.[29–31] The combination of two effects, unquenched orbital momentum,

[a]*Department of Chemistry, National University of Singapore, Block S8 Level 3, 3 Science Drive 3, 117543, Singapore. E-mail: chmlu@nus.edu.sg*
[b]*University of Vienna, Institute of Organic Chemistry, Währinger Strasse 38, A-1090 Vienna, Austria*
[c]*Chemistry Department, College of Science, King Saud University, P.O. Box 2455, Riyadh 11451, Saudi Arabia*
[d]*University of Vienna, Institute of Inorganic Chemistry, Währinger Strasse 42, A-1090 Vienna, Austria. E-mail: Vladimir.Arion@univie.ac.at*
[e]*Theory of Nanomaterials Group, Katholieke Universiteit Leuven, Celestijnenlaan 200F, B-3001 Leuven, Belgium. E-mail: Liviu.Chibotaru@kuleuven.be*

†Electronic supplementary information (ESI) available: Computational details, the full energy spectrum of [$Os^{IV}Cl_4$(Hind)$_2$], images of the active orbitals, results of the calculations for the octahedral and axially distorted $[OsCl_6]^{2-}$ anions. See DOI: 10.1039/d1dt01558c

and strong exchange interaction, was predicted to be a direct route for the design of efficient SMMs, for which complexes of 4d and 5d metal ions would be most rational building blocks.[32]

In this article, we get a new insight into the magnetism of Os^{IV} complexes through the investigation of a recently synthesised *trans*-$[Os^{IV}Cl_4(\kappa N_1\text{-Hind})_2]$, where Hind = 2*H*-indazole,[33] along with two model$[Os^{IV}Cl_6]^{2-}$ complexes. Explicitly correlated *ab initio* calculations show that the low-lying spin–orbit multiplets are well described by the total angular pseudo-momentum $\tilde{J}$ arising from the spin–orbit coupling of the total spin and orbital pseudo-momentum at the Os(IV) ion. In particular, a strong deviation from the octahedral symmetry of the ligand environment of osmium ion does not preclude the $\tilde{J} = 0$ character of the non-magnetic ground state. A crucial role of spin–orbit admixture of highly excited ligand-field and charge-transfer states for the magnetic properties of Os(IV) complexes is inferred.

Computational details

Ab initio single-point calculations were performed on the crystal structure of the *trans*-$[Os^{IV}Cl(\kappa N_1\text{-Hind})_2]$ neutral complex.[33] Fig. 1 shows the structure of the calculated molecule. No computational optimisation of the experimental geometry was performed. All *ab initio* multiconfigurational calculations were performed with the MOLCAS 8.2 program package.[34,35] All energies were calculated by a multi-state second-order perturbation approach (MS-CASPT2) based on a multiconfigurational reference wave function (CASSCF).[36,37] Basis functions describing all atoms were atomic natural orbitals with relativistic core correction (ANO-RCC) type,[38] available by default in the MOLCAS package.

Three types of basis set contractions denoted A (small), B (medium), and C (large) were employed in order to test the influence of the size of the basis set on our results. The contractions of the employed basis sets are given in Table S1.† For the sake of brevity, only the results obtained with the largest basis set C are shown in the text, while the results obtained with basis sets A and B are given in the ESI.†

The Cholesky decomposition[39] of two-electron integrals was not employed, given the relatively small dimension of the compound. Since the accuracy of the multiconfigurational methods relies strongly on the choice of the active space, two reasonably large and computationally affordable active spaces were employed. The first active space denoted AS1 (8 electrons in 12 orbitals) included five 5d orbitals (t_{2g} and e_g) orbitals of the osmium together with their "double shell" and two doubly occupied molecular ligand type orbitals. The included ligand-type orbitals have a dominant contribution from the 3p orbitals of the chlorine (≈70%) hybridised strongly with the 5d orbitals of the Os(IV).[40] This active space already includes most of the static correlation. However, for an accurate description of charge-transfer states, it is not sufficient. The enlarged active space, AS2 (14 electrons in 13 orbitals), was based on the AS1 modified as follows: three doubly occupied ligand type orbitals were added to the active space, while the "double shell" of the e_g shell (two orbitals of mainly 6d′ character) was removed, in order to ensure computational feasibility. The removal of the second shell for the e_g orbitals is supposed to have only a minor effect on the computed low-lying electronic states since in most of these states (triplet and singlet), the e_g shell is not populated. The three ligand type orbitals of the AS2, included in addition to AS1 have the dominant 3p character of the chlorine atoms, while the Os(IV) character is smaller (≈1–10%). This active space included all orbitals which have more than 1% Os 5d character.

All CASSCF wave functions and energies were obtained in state-average calculations. Since the optimisation of the wave function is strongly dependent on the number of excited states optimized for each symmetry and spin multiplicity, we have optimized onlythe roots arising from the lowest "octahedral" terms: ^5E, $^3T_1$, $^1T_1$, ^1E and ^1A. The dynamical electron correlation was added by the complete active space second-order perturbation method – CASPT2. In all CASPT2 calculations, the following orbitals were correlated: 4f, 5s, 5p of Os, 3s, 3p of Cl, 2s, 2p of C, and N. An imaginary shift of 0.1 Ha was added in order to exclude any possible "intruder state" problems. Relativistic effects are known to be highly important for heavy elements, and osmium is not an exception. In MOLCAS, relativistic effects are treated in two steps, based on the decomposition of the Douglas–Kroll Hamiltonian[41–43] in two parts: scalar relativistic effects and the spin–orbit coupling. Scalar relativistic effects are taken into account at the CASSCF level, provided that the relativistic correction of the core electrons is included in the basis set generation. The employed ANO-RCC basis sets already contain scalar relativistic correction.[38] The second step includes the spin–orbit coupling, which is done in MOLCAS by the restricted active space state interaction (RASSI) program,[37,44] which uses CASSCF functions (and CASPT2 energies, if available) as input states.[37,45] In all calculations, the spin–orbit coupling was computed on the basis of all states available from CASSCF/CASPT2 calculations. Temperature dependence of the magnetic susceptibility and the *g* tensors of different Kramers doublets were computed within the SINGLE-ANISO module,[46] implemented recently in MOLCAS 8.2. The same computational approach was applied to investigate two model octahedral complexes $[OsCl_6]^{2-}$ whose structural details are given in the ESI.† The time-dependent density functional theory (TD-DFT) calculations were performed with

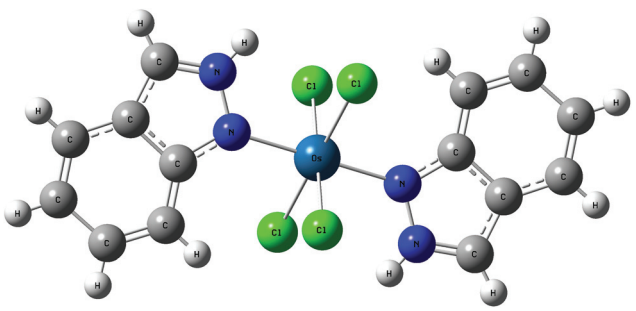

Fig. 1 Structure of the calculated *trans*-$[Os^{IV}Cl_4(\kappa N_1\text{-Hind})_2]$ complex.[33]

the ORCA 4.2 program.[47] All atoms were described by Split-Valence with Polarization (SVP) basis sets developed in the ORCA group.[48]

Magnetic measurements

Details about the synthesis of the investigated compound are given in the ESI.† Magnetic data were obtained with a Quantum Design MPMS SQUID susceptometer. Magnetic susceptibility measurements were performed in the 2–300 K temperature range under a 0.1 T applied magnetic field and diamagnetic corrections were applied by using Pascal's constants.[49]

2 Results and discussion

The Os^{4+} ion in the *trans*-[$Os^{IV}Cl_4(\kappa N_1\text{-Hind})_2$] complex lies in a compressed octahedral environment. All chloride ligands, due to inversion symmetry of the complex, are coplanar and form an almost perfect square. The nitrogen atoms are situated much closer to the osmium than chlorine atoms (by *ca.* 0.29 Å, Fig. 2). As a result, the first coordination sphere of the complex is close to square-bipyramidal (D_{4h}) symmetry (Fig. 2).

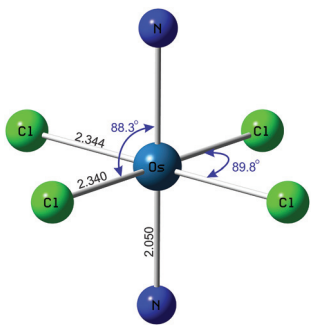

Fig. 2 Structural details of the first coordination sphere of the *trans*-[Os^{IV} $Cl_4(\kappa N_1\text{-Hind})_2$] complex. Interatomic distances are in Ångström. Structures of the calculated $[OsCl_6]^{2-}$ are shown in Fig. S2.†

The energies of the lowest spin states obtained in CASSCF/CASPT2 calculations are shown in Table 1. Similar calculations by a completely different method, TD-DFT, give close values (Table 1) thus proving the reliability of *ab initio* calculations. To get more insight into the nature of obtained molecular terms, similar calculations have been done for a tetragonally distorted octahedral anion $[OsCl_6]^{2-}$ (Fig. S1†). In all calculations, we find the spin-triplet $S = 1$ in the ground state. This state originates from the octahedral orbital triplet $^3T_1$ (Scheme 1) which splits in an orbital singlet (^3A) and an excited orbital doublet (^3E) in D_{4h} symmetry group. The energy separation between ^3A and ^3E is proportional to the strength of the low-symmetry axial components of the ligand field. The similarity of the energy spectrum of two complexes suggests that the tetragonal component is positive ($\Delta_t > 0$). However, the ligand field is not perfectly tetragonal but includes also a rhombic component which is the reason for a slight splitting of the orbital doublet ^3E is (Scheme 1).

The latter appears through small deviations of the geometry of the first coordination sphere from tetragonal (Fig. 2) and due to non-axial symmetry of the Hind ligands. This mainly comes from the presence of a single π orbital at the nitrogen atom (perpendicular to the plane of the Hind ligand) contributing directly to the rhombic component of the crystal field at Os(IV). The relatively small value of the rhombic component evidenced by the splitting of tetragonal E term (Table 1) corroborates the known fact of negligible values for the e_π AOM parameter for the nitrogen of amine ligands or ammonia (see *e.g.*, Fig. 8.19 and section 8.4.1 in ref. 50).

Next, to spin triplets, the lowest excited states are spin singlets, arising from octahedral terms $^1T_2$, ^1E and $^1A_1$. As in the case of the ground octahedral term $^3T_1$, the orbital degeneracy of spin singlets is also removed. Their energy seems to be very sensitive to the dynamical correlation (*cf.* Table 1), which is to be expected, since the 5d orbitals are quite diffuse, and as a result, they have a stronger hybridisation with the ligand's orbitals than the 3d or 4f shells of the metal ions. We can infer

Table 1 Energies (in cm^{-1}) of the calculated spin-free states of the *trans*-[$Os^{IV}Cl_4(\kappa N_1\text{-Hind})_2$] complex and of the distorted-$[Os^{IV}Cl_6]^{2-}$ anion

	trans-[$Os^{IV}Cl_4(\kappa N_1\text{-Hind})_2$]						$[Os^{IV}Cl_6]^{2-}$			
	CASSCF		CASPT2		TD-DFT		CASSCF		CASPT2	
MS	AS1	AS2	AS1	AS2	B3LYP	PBE0	AS1	AS2	AS1	AS2
5	21 932	22 304	21 724	21 214	22 036	23 818	16 366	16 212	15 517	15 858
	26 789	27 221	25 558	26 059	23 240	24 685	29 099	29 016	25 921	25 566
3	0	0	0	0	0	0	0	0	0	0
	3799	3674	4370	3998	3754	4223	3285	2774	4269	3140
	4269	4497	4596	4154	4613	5020	3285	2774	4269	3140
1	8481	7438	5090	4558	3784	5415	7495	6641	4222	4107
	8756	7632	5466	5074	4906	6396	7907	7015	4569	4355
	12 591	11 429	8357	7448	5786	7342	11 261	10 119	7403	6814
	12 862	12 246	9570	8779	8418	10 496	11 261	10 119	9106	7560
	13 117	12 363	9857	9440	17 529	20 340	11 563	10 457	9106	7560
	23 726	21 041	19 273	15 958	18 770	21 178	22 459	21 823	19 540	19 347

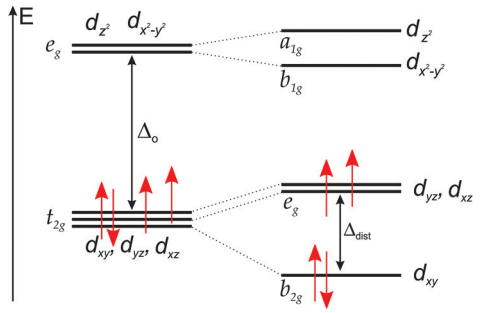

Scheme 1 Splitting of the d orbitals upon symmetry lowering from O_h to D_{4h}, depicted for the case of a tetragonally compressed octahedron (along axis *z*). In the case of an elongated octahedron, the crystal field Δ_t has an opposite sign and, as a result, the e_g and b_{2g} orbitals are reversed. The electronic population in the right plot corresponds to the main electronic configuration of the ground state term ^{3}A. The lowest excited term ^{3}E arises from one-electron transfer $d_{xy} \rightarrow d_{yz}, d_{xz}$.

from the comparison of the energies in Table 1 that the singlets acquire lower excitation energy when the dynamical correlation is included. However, this energy lowering is not sufficient to place the spin-singlet in the ground state. The singlet states correspond to the following genealogy (in order of increasing their energy): $^1T_2 \rightarrow {}^1E + {}^1B_2$, $^1E \rightarrow {}^1A_1 + {}^1B_1$, $^1A_1$.

Finally, the highest in energy are the quintet states corresponding to a complete unpairing of four electrons in the 5d shell. The lowest of them, shown in Table 1, corresponds to one-electron transfer from d_{xy} into $d_{x^2-y^2}$, d_{z^2} orbitals (Scheme 1).

It is worth mentioning here that the doubly occupied ligand type orbitals are close in energy to the 5d orbitals of the Os^{4+}. As a result of this proximity and due to diffuse 5d orbitals, there is a strong mixing between ligands orbitals (3p of chlorine and 2p of the nitrogen) and the 5d orbitals of the Os^{4+}. This hybridisation leads to a large number of ligand-to-metal charge transfer states. We see in Fig. S2† that orbitals 60–64 are mainly of ligand type, in which the contribution of the 5d orbitals of the Os is also significant. These ligand-to-metal charge transfer states are admixed to the ground state *via* the spin–orbit coupling, which is very strong for heavy elements like Os, leading to a strong effect on the temperature-independent paramagnetism. This effect is quite common for many heavy transition metals and actinide compounds.[51,52]

The entire spin–orbit energy spectrum is given in Table S2,† while the energies of the nine low-lying states are also shown in Table 2. We can see that the ground state is well separated from the first excited state, with an energy gap of more than 1500 cm^{-1} in all computational approximations.

2.1. *Ab initio* analysis of low-lying multiplets

Compared to spin states the spectrum of spin–orbital multiplets is significantly reconstructed because the spin–orbit coupling becomes operative in the first order of perturbation theory. Scheme 2 shows the genealogy of low-lying multiplets.

Table 2 Lowest spin–orbit multiplets of the *trans*-$[Os^{IV}Cl_4(\kappa N_1\text{-Hind})_2]$ complex and of the distorted-$[OsCl_6]^{2-}$ anion (in cm^{-1})

trans-$[Os^{IV}Cl_4(\kappa N_1\text{-Hind})_2]$				$[Os^{IV}Cl_6]^{2-}$			
CASSCF/RASSI		CASPT2/RASSI		CASSCF/RASSI		CASPT2/RASSI	
AS1	AS2	AS1	AS2	AS1	AS2	AS1	AS2
0	0	0	0	0	0	0	0
2073	1889	2244	2210	2138	2158	2270	2352
2134	1983	2269	2238	2138	2158	2270	2352
4975	4859	5573	5211	4829	4571	5828	5064
6056	5823	6225	5909	5981	5899	5922	5604
6723	6420	6411	6021	6565	6142	6255	5845
7078	6950	6664	6251	6565	6287	6577	6191
7303	7024	7104	6776	6641	6306	7212	6478
7391	7106	7257	6869	6771	6306	7212	6478

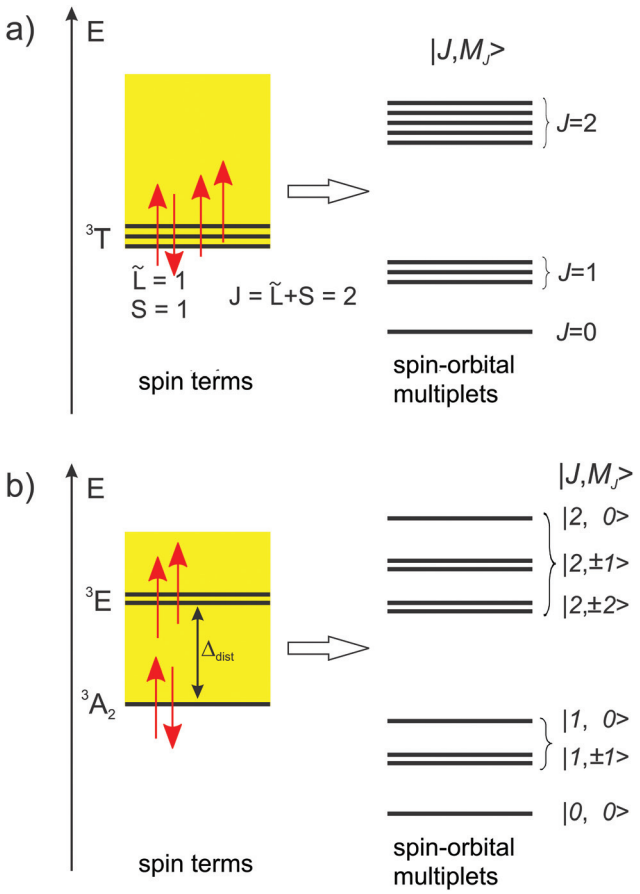

Scheme 2 Spin–orbit coupling effects for the $^3T_1$ term in *trans*-$[Os^{IV}Cl_4(\kappa N_1\text{-Hind})_2]$ complex. (a) In idealised octahedral symmetry and (b) with additional axial ligand field which matches the situation in *trans*-$[Os^{IV}Cl_4(\kappa N_1\text{-Hind})_2]$. The yellow rectangle shows the relative strength of the spin–orbit coupling parameter of the Os^{4+} ion. The positive sign of the $\Delta_{dist} > 0$ corresponds to a compressed octahedron.

In a perfect octahedron the effective angular momentum of the ground $^3T_1$ orbitally degenerate triplet is $\tilde{L} = 1$.[12,25] Due to spin–orbit coupling, neither $\tilde{L}$, nor S is conserved but, only the

total (pseudo) angular momentum $\tilde{J} = \tilde{L} + S$. Since the ground state spin is $S = 1$, the possible values for this total angular momentum are $\tilde{J} = 2, 1, 0$, while the energy separation between the corresponding multiplets is proportional to their total angular momentum (Landè interval rule). This coupling scheme is also kept when the ground orbital triplet $^3T_1$ is slightly split into non-degenerate levels, as long as the spin–orbit coupling remains stronger than this splitting. Obviously, in these situations octahedral $\tilde{J}$-multiplets will be split too. This is exactly the case which we observe for *trans*-[$Os^{IV}Cl_4(\kappa N_1$-Hind)$_2$] compound (Scheme 2). Spin–orbit admixture of other molecular terms modifies this picture to some extent as discussed below.

Expectation values of the angular and total magnetic moments in the low-lying $\tilde{J}$-states of the *trans*-[$Os^{IV}Cl_4(\kappa N_1$-Hind)$_2$] compound are given in Table 3. We notice significant magnetic anisotropy of the excited manifolds.

2.1.1 Effect of spin–orbit admixture of excited terms on the low-lying multiplets. To understand the factors influencing the magnetic properties of the low-lying multiplets in this compound, we analyse in detail the case of the octahedral $[Os^{IV}Cl_6]^{2-}$ anion (Fig. S1†). Fig. S4† shows that the equilibrium geometry is achieved for the Os–Cl distance of 2.40 Å, which is only considered in further calculations. Given a very strong spin–orbit coupling on the Os^{4+} ion the quality of its treatment depends essentially on the number of spin states included in the spin–orbit mixing. To quantify this influence, we performed a series of *ab initio* calculations by admixing a gradually increasing number of spin states. Fig. 3 shows the obtained dependence. We notice the strict conformity to the Landè interval rule when only the ground $^3T_1$ term is included (the first nine states in Fig. 3) in the spin–orbit mixing. Including the excited spin states in the spin–orbit coupling leads to a stronger energy stabilisation of the $\tilde{J} = 0$ state, and to diminishing of energy difference between $\tilde{J} = 1$ and $\tilde{J} = 2$ multiplets. This effect is due to a different admixture of the higher spin states by the spin–orbit coupling to the nine low-lying spin–orbital states.

The analysis shows that allowing mixing with $^1T_2$ lowers the $M = -1, 0, 1$ components of $J = 2$ multiplet resulting in its splitting in threefold and twofold degenerate multiplets in octahedral symmetry (under tetragonal distortion the former further splits into $M = \pm1$ and 0 multiplets, Scheme 2). Admixing the next excited spin singlet ^1E substantially lowers the $M = -2, 2$ components of $J = 2$, thus reducing the splitting of this multiplet. Including the highest spin singlet of the t_{2g}^4 configuration, ^1A, substantially lowers the $J = 0$ multiplet. Including the ^5E term, arising from $t_{2g} \rightarrow e_g$ electron transfer (Scheme 1), lowers all nine state of the low-lying multiplets (Scheme 2), whereas the $J = 2$ components come closer to each other. Finally, including other terms of the $5d^4$ configurations in the spin–orbital mixing mainly lifts the $J = 1$ multiplet with respect to the others. This behavior is found in qualitative agreement with phenomenological ligand-field description.[53–55]

The extent of the spin–orbital admixture of excited terms is seen in Fig. 3b, showing a lowering of the weight of the $^3T_1$ term in the resulting spin–orbital states when the number of mixed states increases. We may conclude that the different weight of this admixture for different spin–orbital states is the reason for the violation of Landè interval. Nevertheless, the weight of the $^3T_1$ term remains very high for any number of states involved in the spin–orbital mixing, which means that the low-lying multiplets can still be characterized by $\tilde{J}$ very much as the molecular orbitals in the ligand-field description are associated with the corresponding d orbitals of the metal ion. This picture remain valid for non-octahedral complexes two, in which case some of the $\tilde{J}$ multiplets become mixed (as, *e.g.*, $M = \pm1$ and $M = \pm2$ component in tetragonal complexes Scheme 2b).

2.1.2 Effect of spin–orbit admixture of higher terms on magnetic properties of low-lying multiplets. The extent of spin–orbit admixture of excited terms has a strong influence on the eigenvalues of the angular and magnetic moments and g factors in the low-lying $\tilde{J}$-states. Fig. 4 shows the comparison of the radial (Os–Cl) dependence of the *ab initio* calculated g factor for the octahedral $[Os^{IV}Cl_6]^{2-}$ anion for the $\tilde{J} = 1$ and $\tilde{J} =$

Table 3 Expectation values of the spin $\langle S_\alpha \rangle$, orbital $\langle L_\alpha \rangle$ and total magnetic $\langle \mu_\alpha \rangle$ moments (in μ_B)) in the low-lying $\tilde{J}$-states of the *trans*-[$Os^{IV}Cl_4(\kappa N_1$-Hind)$_2$] compound (model CASSCF/RASSI, AS2)

	$\|0, 0\rangle$	$\|1, -1\rangle$	$\|1, 0\rangle$	$\|1, +1\rangle$	$\|2, -2\rangle$	$\|2, -1\rangle$	$\|2, 0\rangle$	$\|2, +1\rangle$	$\|2, +2\rangle$
$\langle S_X \rangle$	0.000	0.276	0.000	−0.276	0.888	0.679	0.000	−0.679	−0.888
$\langle L_X \rangle$	0.000	−0.449	0.000	0.449	−0.648	−0.271	0.000	0.271	0.648
$\langle \mu_X \rangle$	0.000	−0.103	0.000	0.103	−1.130	−1.088	0.000	1.088	1.130
$\langle S_Y \rangle$	0.000	−0.157	0.000	0.157	0.862	0.421	0.000	−0.421	−0.862
$\langle L_Y \rangle$	0.000	0.714	0.000	−0.714	−0.523	−0.288	0.000	0.288	0.523
$\langle \mu_Y \rangle$	0.000	−0.399	0.000	0.399	−1.203	−0.555	0.000	0.555	1.203
$\langle S_Z \rangle$	0.000	0.901	0.000	−0.901	−0.072	0.561	0.000	−0.561	0.072
$\langle L_Z \rangle$	0.000	0.091	0.000	−0.091	0.829	−0.721	0.000	0.721	−0.829
$\langle \mu_Z \rangle$	0.000	−1.713	0.000	1.713	−0.685	−0.403	0.000	0.403	0.685

The deviation of the values of momenta for $\tilde{J} = 2$, $M = \pm2$ and $M = \pm1$. The fact that the moments for $M = \pm2$ are not twice the values of the corresponding $M = \pm1$ is due to the presence of higher rank ($k = 3$) irreducible tensor operators (ITOs) entering the decomposition of the momenta for $\tilde{J} = 2$. (The calculated values for rank three ITOs are given in ESI.†)

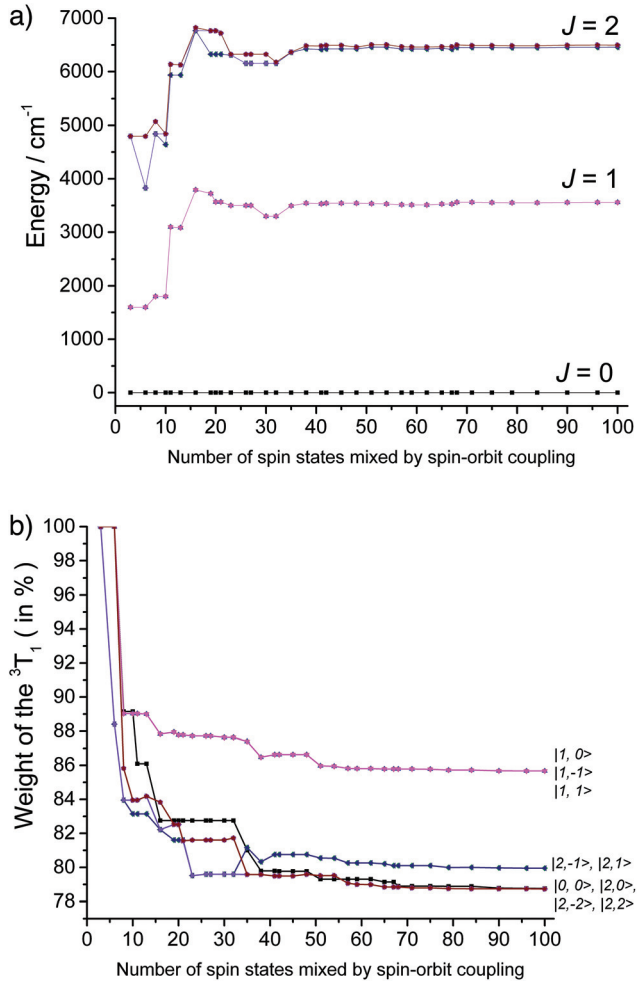

Fig. 3 (a) The influence of the number of spin states mixed by spin–orbit coupling on the energy of low-lying multiplets. Note the strict conformity to the Landè interval rule when only the ground $^3T_1$ is mixed by the spin–orbit coupling (left-hand side of the plot), and the strong deviations from the Landè interval rule when all ligand-field states are considered in the spin–orbit coupling. (b) The weight of the $^3T_1$ term in the wavefunctions of low-lying multiplets (in %). The decrease of the weight of the $^3T_1$ term is due to the admixture of higher excited spin states *via* spin–orbit interaction. The calculations correspond to the octahedral $[Os^{IV}Cl_6]^{2-}$ anion, and are done for the basis set C. Lines are just guide for the eye.

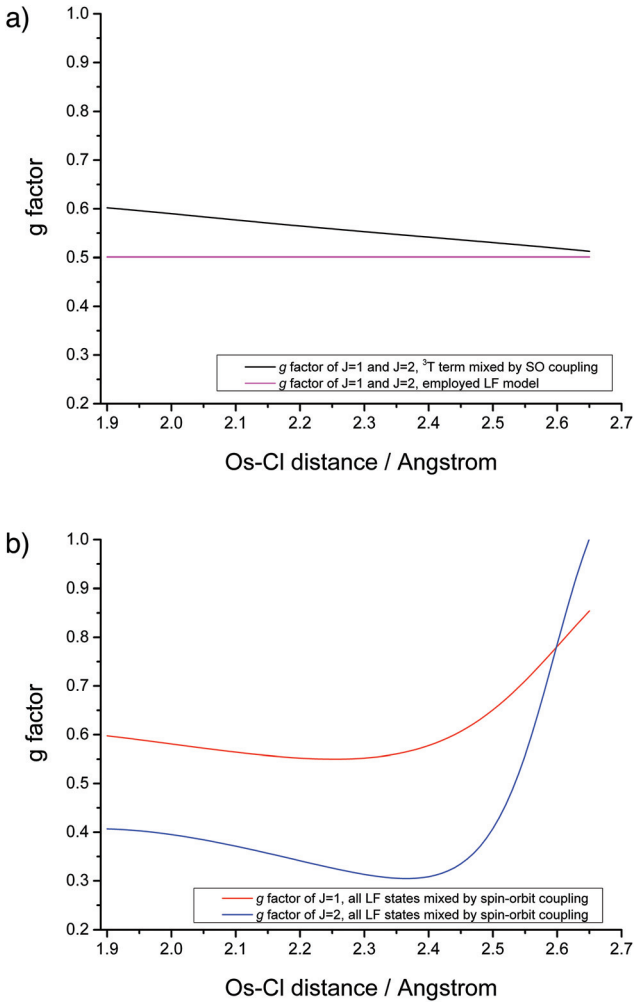

Fig. 4 Evolution of the *g* factor of the $\tilde{J}$ = 1 and $\tilde{J}$ = 2 manifolds of the octahedral $[Os^{IV}Cl_6]^{2-}$ anion as function of the Os–Cl distance. Note the great difference of the *g* factors for $\tilde{J}$ = 1 and $\tilde{J}$ = 2 when only $^3T_1$ states (a) and all ligand-field states (b) are considered in the spin–orbit mixing.

2 multiplets including in the spin–orbit mixing either the ground $^3T_1$ term only or all ligand-field states. The phenomenological ligand-field theory confined to the $^3T_1$ term predicts the same value of the *g* factor for both $\tilde{J}$ multiplets (eqn (S11)†). However, as we can see in Fig. 4a, the shorter the Os–Cl distance in octahedral $[Os^{IV}Cl_6]^{2-}$ anion, the stronger is the deviation from the predictions of the ligand-field theory, due to stronger covalency effects (shorter Os–Cl bond favours stronger covalent bonding). The second and more important effect is the contribution of the excited spin terms to the modifications of orbital, spin and magnetic momenta in the low-lying multiplets (Fig. S6–S8†). This is also seen in the calculated *g* factors when all ligand-field terms arising from the d^4 configuration are considered in the spin–orbit coupling (Fig. 4b), showing a completely different radial dependence compared to the casewhen only the ground $^3T_1$ term was involved (Fig. 4a).

The spin–orbital admixture of higher excited terms to the low-lying multiplets is also responsible for a strong reduction of the *g* factor of the $\tilde{J}$ = 2 manifold compared to the *g* factor of the $\tilde{J}$ = 1 multiplet as it is observed in Fig. 4b. This is because, according to Fig. 3b, the components of the $\tilde{J}$ = 1 multiplet have the weakest spin–orbit contribution from the excited spin states, while states corresponding to the $|0, 0\rangle$, $|2, \pm2\rangle$, and $|2, 0\rangle$ acquire almost 18–22% contribution from the later. The most important admixture comes from excited ^5E, ^1T and ^1E states. Within the employed ligand-field model we cannot take this influence into account explicitly. Clearly the conventional ligand-field model, especially, when confined to the ground term, is not able to describe these effects, nor the magnetism of such complexes. Therefore, the spin–orbital admixture of

the excited terms is very important for a decent description of all properties of low-lying multiplets of Os(IV) and probably of other heavy 5d metals as Ta, Ir, Pt, W, and Re.

2.2 *Ab initio* calculation of the magnetism of $[Os^{IV}Cl_6]^{2-}$ and *trans*-$[Os^{IV}Cl_4(\kappa N_1\text{-Hind})_2]$

2.2.1 Effect of spin–orbit coupling to excited terms on the room temperature magnetic susceptibility. We have seen in the previous section that the ground state of $[Os^{IV}Cl_6]^{2-}$ anion and *trans*-$[Os^{IV}Cl_4(\kappa N_1\text{-Hind})_2]$ complex is non-magnetic, and is strongly influenced by the size of the spin–orbit coupling matrix. The observed magnetic susceptibility in these compounds arises due to temperature independent paramagnetism (TIP), when the diamagnetic ground state admixes the excited ligand-field and charge-transfer states first by strong spin–orbit coupling and subsequently *via* the Zeeman interaction.

Fig. 5 shows the influence of the extent of the spin–orbit mixing on the calculated room temperature magnetic susceptibility. As we can see, the more spin terms are mixed by the spin–orbit coupling the lower is the high-temperature magnetic susceptibility, which is caused mainly by the increase in the energy separation between the ground $\tilde{J} = 0$ and first excited $\tilde{J} = 1$ manifold (see Fig. 3).

Fig. 6 shows the radial dependence of χT at 300 K for the $[Os^{IV}Cl_6]^{2-}$ anion. The experimental value of the magnetic susceptibility of K_2OsCl_6, in which Os^{4+} ion has a perfectly octahedral environment, is 0.28 cm^3 K mol^{-1} (section 9.8.3, Table 9.7 in ref. 50). We notice that the calculated χT at 300 K for the experimental Os–Cl distance in K_2OsCl_6, (0.232 cm^3 K mol^{-1}, Fig. 6) is slightly lower than the experimental one, which means that there are additional effects not considered in our calculation.

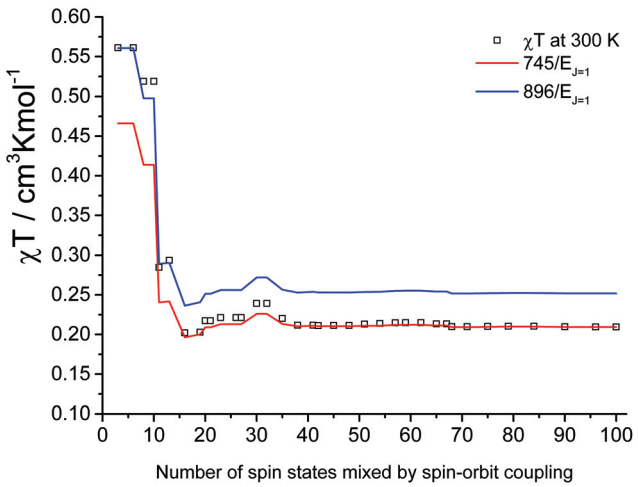

Fig. 5 Evolution of the calculated molar magnetic susceptibility χT at 300 K (square) of the octahedral $[Os^{IV}Cl_6]^{2-}$ anion as function of the number of ligand-field spin states mixed by spin–orbit coupling in RASSI. The red and blue lines represent the value of const/$E_{J=1}$ functions, showing the inverse dependence of the calculated magnetic susceptibility on the energy of the low-lying $J = 1$ manifold ($E_{J=1}$).

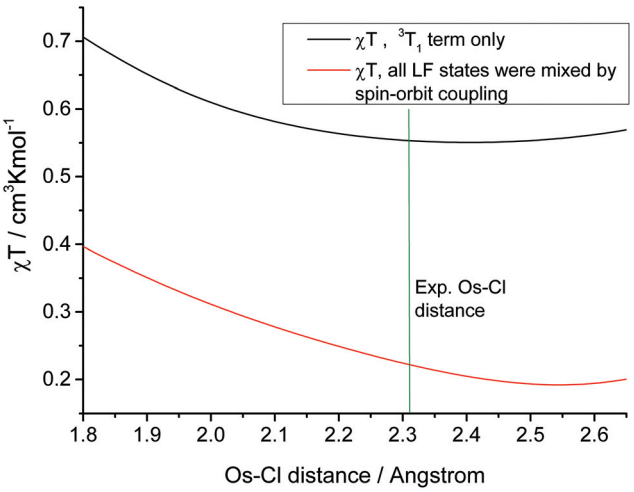

Fig. 6 Radial dependence of the calculated molar magnetisation at 300 K for the octahedral $[Os^{IV}Cl_6]^{2-}$ anion in two limiting cases of treatment of the spin–orbit coupling. Experimental Os–Cl is 2.321 Å.[56]

2.2.2 Influence of the size of active space in CASSCF calculations on the room temperature magnetic susceptibility. Another important factor influencing the calculated magnetic susceptibility is the accuracy of the description of covalency effects. For the studied complexes, due to strong separation of the ligand-field states at Os^{4+}, terms corresponding to electron transfer from Cl to Os are not that high in energy. Due to strong hybridisation of Os 5d with ligand's orbitals, the ligand-field terms usually responsible for magnetism are intermixed with the ligand-to-metal charge transfer states. Theoretical account of the latter is a difficult problem. It is usually done *via* enlarging the active space in CASSCF calculations by including the ligand type orbitals having strong hybridization with the metal. Then a large amount of spin states of ligand-field and charge transfer type are considered in the spin–orbit mixing.

To give an account of these effects we have performed a series of calculations on octahedral $[Os^{IV}Cl_6]^{2-}$ for a gradually increasing number of doubly-occupied ligands orbitals in the active space. Due to limited computer power, we optimized only the ground $^3T_1$ term. Fig. 7 shows the resulting dependence of χT at 300 K on the size of the active space.

As we can see, the presence of the doubly occupied ligand's orbitals in the active space leads to an increase of magnetic susceptibility. The reason for that is the increased hybridization to the ligands' orbitals achieved *via* the admixture of the charge-transfer states to the ligand-field ones. This hybridization lowers the effective strength of the spin–orbit coupling in the ground $^3T_1$ term, which in turn leads to lowering of the energy separation to the $\tilde{J} = 1$ and $\tilde{J} = 2$ manifolds thus increasing the TIP.

2.2.3 Effect of spin–orbital admixture of charge-transfer states on low-lying $\tilde{J}$-multiplets and magnetic susceptibility. To check the effect of charge-transfer states on the multiplet spectrum and magnetism, we considered an active space involving the t_{2g}^4 shell only and all doubly occupied 3p orbitals of the

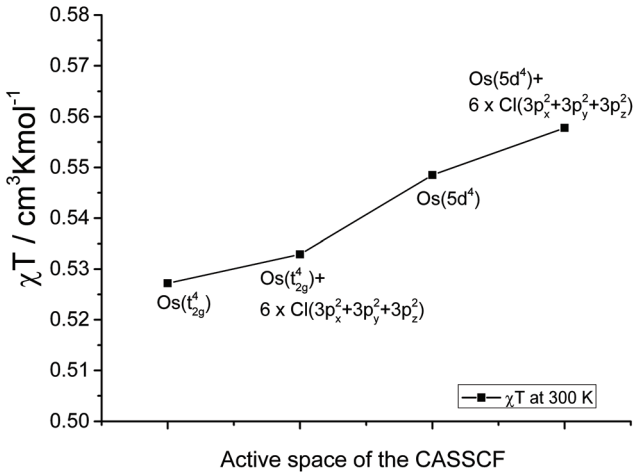

Fig. 7 A comparison of the magnetic susceptibility at 300 K of the $[Os^{IV}Cl_6]^{2-}$ anion calculated for various sizes of the active space of the CASSCF method: inclusion of the ligand orbitals in the active space leads to a more accurate description of the Os–Cl covalency. Only the optimized $^3T_1$ term at CASSCF level was included in the spin–orbit coupling in RASSI.

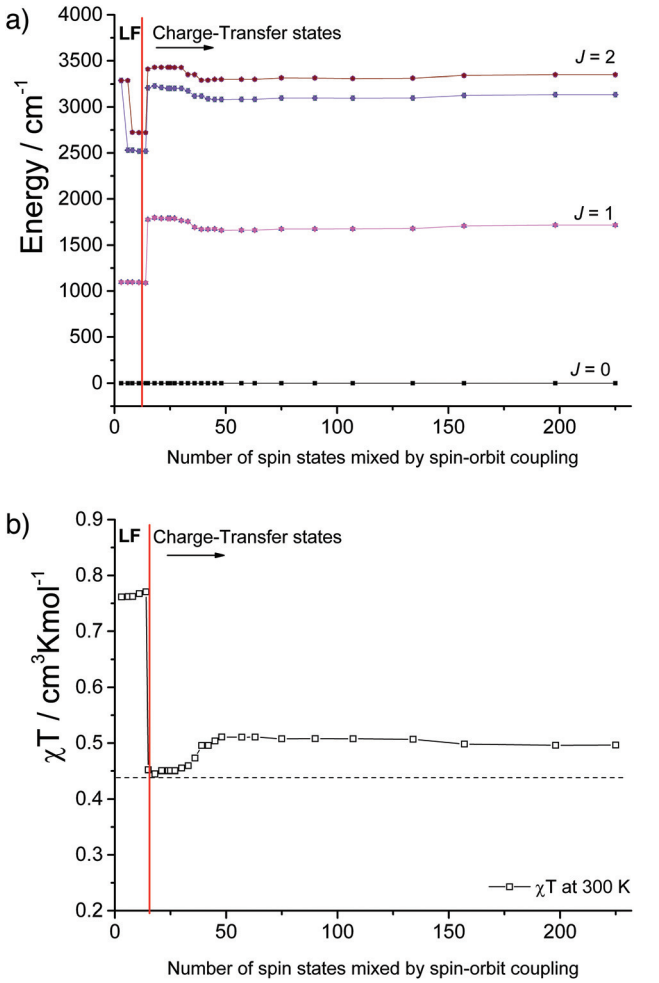

Fig. 8 Influence of the number of states of ligand-field and charge-transfer origin mixed by the spin–orbit coupling on the calculated energy of the low-lying multiplets (a) and on the calculated molar magnetic susceptibility (b) of the $[Os^{IV}Cl_6]^{2-}$ anion. The increase of the χT from the minimal value, obtained when all ligand-field states are considered, is due to the inclusion of charge-transfer states in the spin–orbit coupling (*i.e.* compare with Fig. 5 and 6).

chlorine atoms (CAS(40 in 21)). All triplet spin states and all singlet spin states were optimized at the state-average CASSCF level of theory employing the basis set C. Note that in this active space, there is only a limited number of ligand field states, namely $^3T_1$, $^1T_1$, ^1E, and ^1A, while all other excited states are of charge-transfer type, corresponding to the transfer of one or several electrons from the 3p orbitals of chlorine atoms to the $t_{2g}{}^4$ shell of Os^{IV}. Fig. 8 shows the dependence of the energies of the low-lying multiplets and magnetic susceptibility on the number of charge-transfer states included in the spin–orbit coupling.

We notice that the $\tilde{J} = 1$ and $\tilde{J} = 2$ multiplets acquire much lower excitation energies compared to the case when only ligand-field terms are mixed (Fig. 3). This is because in Fig. 3 a large number of ligand-field states were considered in the spin–orbit mixing, while in Fig. 8 only a small number of them were included. Comparing Fig. 5 and 8b, we see that the admixture of excited ligand-field states causes a large splitting of the $\tilde{J}$-manifolds, leading to a strong decrease of the calculated χT, while further admixture of the charge-transfer states leads to an obvious increase of the calculated magnetic susceptibility from the lowest value. From this analysis we may conclude that the best treatment would imply:

- including all ligand's valence orbitals (3s, and 3p of Cl in the present case) and sufficiently large number of empty orbitals of the metal (6s, 6p, the second shell of 5d orbitals, *etc.*) in the active space;
- optimising the wave functions for a large number of ligand-field and charge-transfer states; preferably performing separate orbital optimisations for the two classes of states;
- including all optimized states in the spin–orbit coupling.

2.2.4 Magnetic susceptibility of *trans*-$[Os^{IV}Cl_4(\kappa N_1\text{-Hind})_2]$. Magnetic susceptibility of the *trans*-$[Os^{IV}Cl_4(\kappa N_1\text{-Hind})_2]$ complex has been measured as described above. Fig. 9 shows the comparison with theoretical predictions in different computational approximations. We can infer that the best agreement is obtained for the largest basis set (C) and the largest active space (AS2) when no dynamical correlation is considered.

As Fig. 9 shows, the increase of the number of ligand orbitals in the active space (AS2 *vs.* AS1) leads to an increase in the calculated magnetic susceptibility. The reason is the same as for $[Os^{IV}Cl_6]^{2-}$ (Fig. 7), the enhancement of the hybridisation of the 5d orbitals with the ligand-type orbitals and the accompanying reduction of the effective spin–orbit coupling interaction. The account of dynamical correlation (the CASPT2 step) has an opposite effect reflected in an increase of the gaps between the low-lying $\tilde{J}$-multiplets, thus reducing the susceptibility (green line in Fig. 9). The account of more ligand-field states is not expected to change significantly the calculated

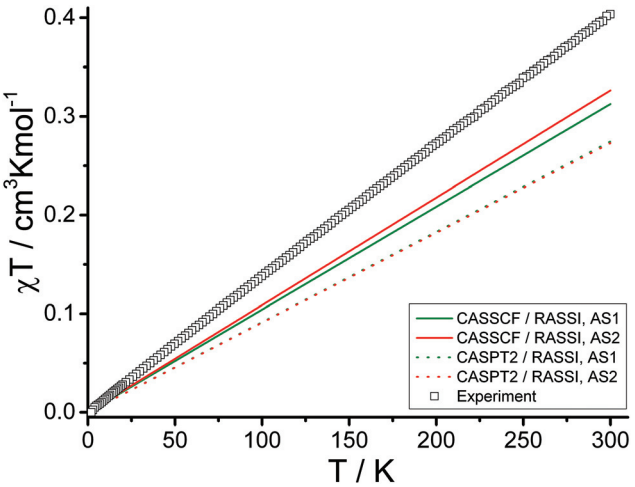

Fig. 9 A comparison between measured (empty squares) and calculated magnetic susceptibility (lines) in different computational approximations.

susceptibility further if one follows the trend observed for $[Os^{IV}Cl_6]^{2-}$ (Fig. 5). Therefore, to recover the discrepancy of *ca.* 30% between the calculated line and measured susceptibility one should probably include the effect of the charge transfer states. Indeed, the analysis in the previous section shows that the account of their admixture increases the calculated χT by 15–20% for $[Os^{IV}Cl_6]^{2-}$ (Fig. 9). Compared to the latter, *trans*-$[Os^{IV}Cl_4(\kappa N_1\text{-Hind})_2]$ has a significantly higher density of charge-transfer states due to more bulky axial ligands. The above analysis shows that at variance to most 3d and 4f complexes, we cannot confine ourselves to ligand-field states when describing the magnetism of osmium complexes, and probably of the entire third transition row metal complexes. For such a purpose the *ab initio* approach becomes indispensable although the required calculations are much more involved and demanding compared to similar treatment if complexes of first transition row metals and lanthanides, as testified by the present calculations.

3 Conclusions

In this work the electronic and magnetic properties of a recently synthesised low-symmetric *trans*-$[Os^{IV}Cl_4(\kappa N_1\text{-Hind})_2]$,[33] and octahedral and tetragonally distorted $[Os^{IV}Cl_6]^{2-}$ were studied by explicitly correlated *ab initio* methods. It is found that despite strong metal–ligand covalency the low-lying multiplets are basically characterized by the total angular pseudo-momentum $\tilde{J}$ originating from the spin–orbit coupling of the ground-state spin with the orbital pseudo-momentum of the Os^{IV} ion. The strong spin–orbit interaction also preserves the dominant $\tilde{J} = 0$ character of the non-magnetic ground state in the *trans*-$[Os^{IV}Cl_4(\kappa N_1\text{-Hind})_2]$ complex despite significant deviation of the ligand environment of Os^{IV} from octahedral symmetry. At the same time the spin–orbit admixture of all multiplets arising from the t_{2g}^4 strong-field electronic configuration is indispensable for the correct description of magnetic properties of Os^{IV} complexes.

We have found that the charge-transfer states have an unexpectedly strong effect on the magnetic properties of investigated Os^{IV} complexes and should be taken into account in order to achieve their quantitative description. This situation is specific for the present and probably other 5d complexes and does not occur in 3d complexes and lanthanides, for which the charge-transfer states have never been advocated in connection with their magnetic properties.[12,25,49] The reason why the charge transfer states become important in the present case is the strong spin–orbit coupling on the osmium ion, which in combination with strong covalency between 5d and ligand orbitals, induce their strong spin–orbital admixture.

Conflicts of interest

There are no conflicts to declare.

Acknowledgements

L. U. acknowledges the financial support of the research projects R-143-000-A65-133 and R-143-000-A80-114 of the National University of Singapore. *Ab initio* calculations were done on the ASPIRE-1 cluster (http://www.nscc.sg) under the project 11001278. This work was supported by the Distinguished Scientist Fellowship Program (DSFP) of King Saud University, Riyadh, Saudi Arabia.

References

1 P. Zhang and P. J. Sadler, *J. Organomet. Chem.*, 2017, **839**, 5–14.
2 S. M. Meier-Menches, C. Gerner, W. Berger, C. G. Hartinger and B. K. Keppler, *Chem. Soc. Rev.*, 2018, **47**, 909–928.
3 M. A. Esteruelas, C. García-Yebra, J. Martín and E. Oñate, *ACS Catal.*, 2018, **8**, 11314–11323.
4 G. Chelucci, *Coord. Chem. Rev.*, 2017, **331**, 1–36.
5 Y. Sasaki, S. Amemori, H. Kouno, N. Yanai and N. Kimizuka, *J. Mater. Chem. C*, 2017, **5**, 5063–5067.
6 X.-Y. Wang, C. Avendaño and K. R. Dunbar, *Chem. Soc. Rev.*, 2011, **40**, 3213–3238.
7 S. V. Streltsov and D. I. Khomskii, *Phys.-Usp.*, 2017, **60**, 1121–1146.
8 X.-L. Sheng and B. K. Nikolić, *Phys. Rev. B*, 2017, **95**, 201402.
9 G. Khaliullin, *Phys. Rev. Lett.*, 2013, **111**, 197201.
10 Y. Shi, Y. Guo, Y. Shirako, W. Yi, X. Wang, A. A. Belik, Y. Matsushita, H. L. Feng, M. Tsujimoto, Y. Arai, N. Wang, M. Akaogi and K. Yamaura, *J. Am. Chem. Soc.*, 2013, **135**, 16507–16516.
11 Z. Y. Zhao, S. Calder, A. A. Aczel, M. A. McGuire, B. C. Sales, D. G. Mandrus, G. Chen, N. Trivedi, H. D. Zhou

and J.-Q. Yan, *Phys. Rev. B: Condens. Matter Mater. Phys.*, 2016, **93**, 134426.
12 J. S. Griffith, *The Theory of Transition-Metal Ions*, Cambridge University Press, Cambridge, 1971.
13 N. Ishikawa, M. Sugita, T. Ishikawa, S.-y. Koshihara and Y. Kaizu, *J. Am. Chem. Soc.*, 2003, **125**, 8694–8695.
14 N. Ishikawa, M. Sugita, T. Ishikawa, S.-y. Koshihara and Y. Kaizu, *J. Phys. Chem. B*, 2004, **108**, 11265–11271.
15 N. Ishikawa, M. Sugita and W. Wernsdorfer, *Angew. Chem., Int. Ed.*, 2005, **44**, 2931–2935.
16 N. Ishikawa, M. Sugita and W. Wernsdorfer, *J. Am. Chem. Soc.*, 2005, **127**, 3650–3651.
17 M. A. AlDamen, J. M. Clemente-Juan, E. Coronado, C. Martí-Gastaldo and A. Gaita-Ariño, *J. Am. Chem. Soc.*, 2008, **130**, 8874–8875.
18 M. A. AlDamen, S. Cardona-Serra, J. M. Clemente-Juan, E. Coronado, A. Gaita-Ariño, C. Martì-Gastaldo, F. Luis and O. Montero, *Inorg. Chem.*, 2009, **48**, 3467–3479.
19 M. Gonidec, F. Luis, À. Vìlchez, J. Esquena, D. Amabilino and J. Veciana, *Angew. Chem., Int. Ed.*, 2010, **49**, 1623–1626.
20 F. Luis, M. J. Martìnez-Pérez, O. Montero, E. Coronado, S. Cardona-Serra, C. Martì-Gastaldo, J. M. Clemente-Juan, J. Sesé and D. D. T. Schurig, *Phys. Rev. B: Condens. Matter Mater. Phys.*, 2010, **82**, 060403.
21 H. L. C. Feltham, Y. Lan, F. Klöwer, L. Ungur, L. F. Chibotaru, A. K. Powell and S. Brooker, *Chem. – Eur. J.*, 2011, **17**, 4362–4365.
22 J. D. Rinehart and J. R. Long, *J. Am. Chem. Soc.*, 2009, **131**, 12558–12559.
23 J. D. Rinehart, K. R. Meihaus and J. R. Long, *J. Am. Chem. Soc.*, 2010, **132**, 7572–7573.
24 K. R. Meihaus, J. D. Rinehart and J. R. Long, *Inorg. Chem.*, 2011, **50**, 8484–8489.
25 A. Abragam and B. Bleaney, *Electron Paramagnetic Resonance of Transition Ions*, Clarendon Press, Oxford, 1970.
26 W. H. Harman, T. D. Harris, D. E. Freedman, H. Fong, A. Chang, J. D. Rinehart, A. Ozarowski, M. T. Sougrati, F. Gean, G. J. Long, J. R. Long and C. J. Chang, *J. Am. Chem. Soc.*, 2010, **132**, 18115–18126.
27 L. F. Chibotaru, M. F. A. Hendrickx, S. Clima, J. Larionova and A. Ceulemans, *J. Phys. Chem. A*, 2005, **109**, 7251–7257.
28 T. D. Harris, C. Coulon, R. Clérac and J. R. Long, *J. Am. Chem. Soc.*, 2011, **133**, 123–130.
29 O. Kahn, J. Larionova and L. Ouahab, *Chem. Commun.*, 1999, 945–952.
30 J. Larionova, O. Kahn, S. Gohlen, L. Ouahab and R. Clérac, *J. Am. Chem. Soc.*, 1999, **121**, 3349–3356.
31 A. Kaur Sra, M. Andruh, O. Kahn, S. Golhen, L. Ouahab and J. V. Yakhmi, *Angew. Chem., Int. Ed.*, 1999, **38**, 2606–2609.
32 V. S. Mironov, L. F. Chibotaru and A. Ceulemans, *J. Am. Chem. Soc.*, 2003, **125**, 9750–9760.
33 G. E. Büchel, I. N. Stepanenko, M. Hejl, M. A. Jakupec, B. K. Keppler and V. B. Arion, *Inorg. Chem.*, 2011, **50**, 7690–7697.
34 F. Aquilante, J. Autschbach, R. K. Carlson, L. F. Chibotaru, M. G. Delcey, L. De Vico, I. F. Galvàn, N. Ferré, L. M. Frutos, L. Gagliardi, M. Garavelli, A. Giussani, C. E. Hoyer, G. Li Manni, H. Lischka, D. Ma, P. Å. Malmqvist, T. Müller, A. Nenov, M. Olivucci, T. B. Pedersen, D. Peng, F. Plasser, B. Pritchard, M. Reiher, I. Rivalta, I. Schapiro, J. Segarra-Martì, M. Stenrup, D. G. Truhlar, L. Ungur, A. Valentini, S. Vancoillie, V. Veryazov, V. P. Vysotskiy, O. Weingart, F. Zapata and R. Lindh, *J. Comput. Chem.*, 2016, **37**, 506–541.
35 F. Aquilante, J. Autschbach, A. Baiardi, S. Battaglia, V. A. Borin, L. F. Chibotaru, I. Conti, M. De Vico, L. Elcey, I. F. Galvàn, N. Ferrè, L. Freitag, M. Garavelli, X. Gong, S. Knecht, E. D. Larsson, R. Lindh, M. Lundberg, P.-A. Malmqvist, A. Nenov, J. Norell, M. Odelius, M. Olivucci, T. B. Pedersen, Q. M. Pedraza-Gonzàlez, L. nd Phung, K. Pierloot, M. Reiher, I. Schapiro, J. Segarra-Martì, F. Segatta, L. Seijo, S. Sen, D. C. Sergentu, C. J. Stein, L. Ungur, M. Vacher, A. Valentini and V. Veryazov, *J. Chem. Phys.*, 2020, **152**, 214117.
36 P.-A. Malmqvist and B. O. Roos, *Chem. Phys. Lett.*, 1989, **155**, 189.
37 P.-Å. Malmqvist, B. O. Roos and B. Schimmelpfennig, *Chem. Phys. Lett.*, 2002, **357**, 230–240.
38 B. O. Roos, R. Lindh, P.-A. Malmqvist, V. Veryazov and P.-O. Widmark, *J. Phys. Chem. A*, 2005, **109**, 6575–6579.
39 F. Aquilante, L. Gagliardi, T. B. Pedersen and R. Lindh, *J. Chem. Phys.*, 2009, **130**, 154107.
40 K. Pierloot, *Mol. Phys.*, 2003, **101**, 2083–2094.
41 M. Douglas and N. M. Kroll, *Ann. Phys.*, 1974, **82**, 89–155.
42 B. A. Hess, *Phys. Rev. A*, 1986, **33**, 3742–3748.
43 M. Reiher, *Wiley Interdiscip. Rev.: Comput. Mol. Sci.*, 2012, **2**, 139–149.
44 B. A. Heß, C. M. Marian, U. Wahlgren and O. Gropen, *Chem. Phys. Lett.*, 1996, **251**, 365–371.
45 B. O. Roos and P.-Å. Malmqvist, *Phys. Chem. Chem. Phys.*, 2004, **6**, 2919–2927.
46 L. Ungur and L. F. Chibotaru, *SINGLE_ANISO module in MOLCAS*, 2007.
47 F. Neese, *Wiley Interdiscip. Rev.: Comput. Mol. Sci.*, 2018, **8**, e1327.
48 D. A. Pantazis, X.-Y. Chen, C. R. Landis and F. Neese, *J. Chem. Theory Comput.*, 2008, **4**, 908–919.
49 O. Kahn, *Molecular Magnetism*, Wiley-VCH, 1993.
50 B. N. Figgis and M. A. Hitchman, *Ligand Field Theory and Its Applications*, Wiley-VCH, 1999.
51 J. Abbenseth, M. Diefenbach, S. C. Bete, C. Würtele, C. Volkmann, S. Demeshko, M. C. Holthausen and S. Schneider, *Chem. Commun.*, 2017, **53**, 5511–5514.
52 F. Gendron, B. Le Guennic and J. Autschbach, *Inorg. Chem.*, 2014, **53**, 13174–13187.
53 H.-H. Schmidtke and D. Strand, *Inorg. Chim. Acta*, 1982, **62**, 153–159.
54 C. D. Flint and A. G. Paulusz, *Mol. Phys.*, 1980, **41**, 907–923.
55 C. van Wüllen, *Mol. Phys.*, 2013, **111**, 2392–2397.
56 R. L. Armstrong, R. M. Morra, I. Svare and B. M. Powell, *Can. J. Phys.*, 1987, **65**, 386–391.

